12th IFAC International Symposium on
Advanced Control of Chemical Processes
July 14-17, 2024. Toronto, Canada

# Inferential Sensors in an Extended Kalman Filter for Fault Estimation ⋆

**Efi Safikou** * **George M. Bollas** **

* *Department of Electrical and Computer Engineering, University of Connecticut, Storrs, CT 06269, USA (e-mail: efstathia.safikou@uconn.edu).*
** *Department of Chemical and Biomolecular Engineering, University of Connecticut, Storrs, CT 06269, USA (e-mail: george.bollas@uconn.edu).*

**Abstract:** Fault estimation is crucial for ensuring reliability and safety throughout industrial processes. However, the increased nonlinearity and complexity in modern systems, as well as their feedback control logic, multiply the challenges when estimating faults. Health monitoring in today's systems may impact the overall cost substantially. To address such challenges, we present a hybrid fault estimation scheme for nonlinear systems, by incorporating an Extended Kalman Filter along with inferential sensors. These fault-sensitive sensors are developed using symbolic regression combined with information theory, to be cost-effective supplements to the existing hard sensors. The proposed method was applied to open-loop and closed-loop architectures of a plate-fin cross-flow heat exchanger dynamic model toward estimating the fault severity at various levels of measurement noise. To showcase the robustness of the inferential sensors, we compared the performance of the proposed framework to an Extended Kalman Filter designed solely with information from hard sensor measurements.

*Keywords:* Fault estimation, Inferential Sensors, Extended Kalman Filter, Symbolic Regresion

## 1. INTRODUCTION

Preventing system faults and failures may lead to significant cost savings. Early fault detection enables organizations to optimize maintenance planning, leading to cost-effective preventive measures and minimizing the necessity for costly emergency repairs. Thus, the demand for advanced system health monitoring algorithms is on the rise. Many research efforts aim to improving fault estimation in complex and nonlinear systems using more sophisticated and cost-efficient algorithms (Mu et al., 2022; Livera et al., 2017; Tan et al., 2021).

Extensive research has been conducted over the years in the field of model-based fault detection methods, which are designed to identify system faults, by leveraging fundamental knowledge of the physical principles governing a system. Kalman filters, for instance, constitute a widely used and robust approach in the field of fault estimation (Glavaški and Elgersma, 2001; Maybeck, 1999; Jihani et al., 2023). Other model-based approaches are proposed in Bokor and Szabó (2009) and Boskovic et al. (1999). In the former the authors used a multiple hypothesis testing method, while in the latter they recommended a methodology that relies on multiple models, switching strategies, and tuning techniques. The effectiveness of these techniques is based on a profound grasp of the underlying physical phenomena, but one of the primary drawbacks is their sensitivity to model uncertainty.

Lately, the increased computational capabilities of modern systems turned the research focus to more advanced techniques, like data-driven and deep learning approaches. These approaches require large quantities of data, from where they derive statistical relationships. Clustering methods and principal component analysis are some of the well-established data-driven approaches for fault identification; see e.g., Lemos et al. (2013); Harmouche et al. (2014). Deep learning schemes, on the other hand, as Neural Networks (NN), have been proven very effective tools in estimating system faults. In Masdoua et al. (2023), Convolutional Neural Networks (CNN) and Long Term Short Memory (LSTM) neural networks were proposed for detecting the faults in Air Handling Unit (AHU) systems, while Sun in Sun et al. (2019) developed an improved Neural Network for fault identification in closed-loop systems. A big challenge of these methods, however, is the absence of a clear understanding of the physical aspects, given that they do not rely on pre-existing knowledge of the system in question.

In this paper, we introduce a framework that merges data-driven and model-based approaches for the purpose of fault estimation, in both open and closed-loop systems. It has been shown that this fusion efficiently harnesses the advantages of both methods while mitigating their individual drawbacks. In detail, we developed an Extended Kalman Filter (EKF) for estimating the fault in the system. Herein, the EKF incorporates data from inferential

⋆ This work was supported by the Pratt & Whitney Institute for Advanced Systems Engineering (P&W-IASE) of the University of Connecticut. Any opinions expressed herein are those of the authors and do not represent those of the sponsor.

sensors, which have been created through the fusion of symbolic regression and information theory techniques. These sensors are designed to provide rich and informative measurements, specifically tailored to enhance the detection of system faults by maximizing sensitivity and neglecting the impact of uncertainty; see e.g., Safikou and Bollas (2021). For method verification, we conducted a performance comparison between the EKF using inferred sensor measurements and the EKF using direct hard sensor measurements.

The paper is structured as follows: in Section II, we present the open-loop and the closed-loop system model, as well as the framework for the creation of the inferential sensors for both structures. The mathematical formulation of fault severity estimation using an Extended Kalman Filter (EKF) is also provided in detail. Section III contains a description of a cross-flow plate-fin heat exchanger system, which we used to apply and test the proposed methodology. In Section IV, we show results on fault estimation, along with comparisons between the existing system sensors and the obtained inferential sensors. Finally, Section V concludes this study.

## 2. METHODS

### *2.1 System Model: An open-loop and a closed-loop structure*

*Open-loop structure:* In this study, the system model $\Sigma$ comprises a set of differential-algebraic equations, which essentially encompass all physical knowledge of the nonlinear system:

$$\dot{\mathbf{x}}(t) = \mathbf{f}(\mathbf{x}(t), \mathbf{u}(t), \boldsymbol{\theta}, t), \tag{1}$$

where $\mathbf{f}$ denotes the system governing equations, while $\mathbf{x}(t)$ and $\dot{\mathbf{x}}(t)$ correspond to vectors of the state variables and their derivatives with respect to time, $t$, respectively. The inputs of the system, $\mathbf{u}(t)$, include the controllable system inputs, $\mathbf{u}_p(t)$, and the uncertain inputs, $\mathbf{u}_q$, while the measured outputs of the system, $\hat{\mathbf{y}}$, are given by $\hat{\mathbf{y}} = \mathbf{h}(\mathbf{x}(t), \mathbf{u}(t), \boldsymbol{\theta}, t)$. The vector $\boldsymbol{\theta}$ consists of the model parameters that represent (i) the faults, $\boldsymbol{\theta}_f$, (ii) the system uncertainty, $\boldsymbol{\theta}_q$, as well as (iii) the system design, $\boldsymbol{\theta}_p$. Note that faults, uncertain parameters, and uncertain inputs are usually the parameters of interest in a fault detection problem. In this regard, we combine them into a new vector, $\boldsymbol{\xi}$, and separate them into the parameters that declare faults, $\boldsymbol{\xi}_f$, and uncertainty, $\boldsymbol{\xi}_q$: $\boldsymbol{\xi} = [\boldsymbol{\theta}_f, \boldsymbol{\theta}_q] \cup [\mathbf{u}_q] = [\boldsymbol{\xi}_f, \boldsymbol{\xi}_q]$.

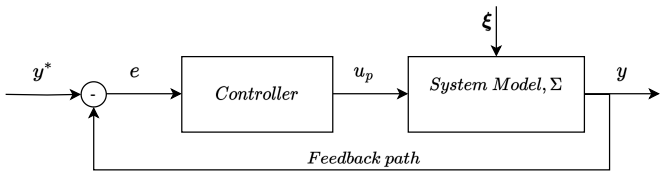


Fig. 1. Schematic of the closed-loop system model.

*Closed-loop structure:* Fig. 1 schematically shows a simple closed-loop system, where $\Sigma$ denotes the model of a nonlinear system (see Eq. 1). For the feedback control logic, we employed a proportional-integral (PI) controller, which estimates the deviation, $e$, of the measured data $y$ from a desired target value $y^*$, and then corrects the control input, $u_p$, in such a way that $y$ remains equal to $y^*$; see e.g., Switzer et al. (1988); Shamsuzzoha (2013). The formulation of the PI controller is given by the following relation:

$$u_p(t) = K_P e(t) + K_I \int_0^t e(t)\, dt, \tag{2}$$

where, $K_P$ and $K_I$ are the non-negative coefficients for the proportional and integral terms, respectively.

For the efficient and accurate estimation of the term $\int_0^t e(t)\, dt$, we augmented the system model of Eq. 1 by adding the error term as a differential equation, i.e., $\dot{x}_e(t) = e$. Thus, by integrating the system, we estimate directly the term $x_e(t) = \int_0^t e(t)\, dt$. This can be achieved easily by transforming the system into symbolic form toward leveraging automatic differentiation (AD) to efficiently construct the sensitivity matrices, $\mathbf{Q}_i^{[l]}$ (see Eq. 3). AD was implemented here using CasADi, an open-source tool for nonlinear optimization and algorithmic differentiation, which allows the user to construct symbolic expressions (Andersson et al., 2012).

### *2.2 Information Theory*

In a fault detection problem, our interest is to gather as much information as possible for faults or other parameters that affect fault identification (such as uncertainty and noise). An effective approach can be based on information theory, and specifically on the Fisher Information Matrix (FIM) (Bar-Shalom et al., 2001). Here, the FIM was employed as a measure of the information related to the parameters of interest $\boldsymbol{\xi}$.

For the estimation of the FIM, we conducted a sensitivity analysis, which reflects the sensitivity of a sensor, $s$, with respect to the different values of $\boldsymbol{\xi}_f$ and $\boldsymbol{\xi}_q$. For $N_{sp}$ timesteps during a timespan, $\boldsymbol{\tau}$, the sensitivity matrix of the $i^{th}$ sensor with respect to $\boldsymbol{\xi}$ is given as follows:

$$\mathbf{Q}_i^{[l]} = \begin{bmatrix} \left.\frac{\partial \hat{s}_i(t_1)}{\partial \xi_1}\right|_{\tilde{\boldsymbol{\xi}}^{[l]}, t_1} & \cdots & \left.\frac{\partial \hat{s}_i(t_1)}{\partial \xi_{N_\xi}}\right|_{\tilde{\boldsymbol{\xi}}^{[l]}, t_1} \\ \vdots & \ddots & \vdots \\ \left.\frac{\partial \hat{s}_i(t_{N_{sp}})}{\partial \xi_1}\right|_{\tilde{\boldsymbol{\xi}}^{[l]}, t_{N_{sp}}} & \cdots & \left.\frac{\partial \hat{s}_i(t_{N_{sp}})}{\partial \xi_{N_\xi}}\right|_{\tilde{\boldsymbol{\xi}}^{[l]}, t_{N_{sp}}} \end{bmatrix}, \tag{3}$$

where, $N_\xi$ is the total number of the parameters of interest, and $\tilde{\boldsymbol{\xi}}^{[l]}$ contains the anticipated values of the fault and uncertain parameters for the $l^{th}$ fault scenario, denoted as $\tilde{\boldsymbol{\xi}}_f^{[l]}$ and $\tilde{\boldsymbol{\xi}}_q^{[l]}$, respectively.

For all $N_l$ studied fault scenarios, $\tilde{\tilde{\boldsymbol{\xi}}}_q^{[l]}$ comprises the mean values of its individual components. On the other hand, a different fault level was adopted for $\tilde{\tilde{\boldsymbol{\xi}}}_f^{[l]}$ in each fault scenario $l$. Specifically, the fault level is known beforehand from past system operation or can be estimated from historical data. Given $\mathbf{Q}_i^{[l]}$, the FIM is derived as shown below:

$$\mathbf{H}_\xi^{[l]}(\tilde{\boldsymbol{\xi}}^{[l]}) = \frac{\sum_{i=1}^{N_s} \sigma_i^{-2} {\mathbf{Q}_i^{[l]}}^T \mathbf{Q}_i^{[l]}}{N_s}, \tag{4}$$

where, $N_s$ is the total number of the incorporated sensors and $\sigma_i^2$ is the measurement variance of the $i^{th}$ sensor.

The development of various optimality criteria are founded on the FIM. Such criteria include the A-optimality, D-optimality, as well as the $D_s$-optimality; see also Atkinson (2011). For this study, the $D_s$-optimality criterion was the most appropriate, as a subset (i.e., $\boldsymbol{\xi}_f$) of $\boldsymbol{\xi}$ needs to be estimated. The $D_s$-optimality criterion achieves fault isolation by eliminating the covariance between the parameters related to faults and uncertainty, while simultaneously providing improved detection outcomes by neglecting the covariance between the elements that identify uncertainty; see Palmer and Bollas (2019). It is formulated by partitioning the FIM into three sub-matrices, as follows:

$$\mathbf{H}_{\xi}^{[l]}(\tilde{\boldsymbol{\xi}}^{[l]}) = \begin{bmatrix} \mathbf{H}_{ff}^{[l]} & \mathbf{H}_{fq}^{[l]} \\ \mathbf{H}_{qf}^{[l]} & \mathbf{H}_{qq}^{[l]}, \end{bmatrix} \tag{5}$$

$$\begin{aligned} &\mathbf{H}_{ff}^{[l]} \in \mathbb{R}^{N_f \times N_f}, \quad \mathbf{H}_{fq}^{[l]} \in \mathbb{R}^{N_f \times (N_\xi - N_f)}, \\ &\mathbf{H}_{qf}^{[l]} = (\mathbf{H}^{[l]})_{fq}^{T}, \quad \mathbf{H}_{qq}^{[l]} \in \mathbb{R}^{(N_\xi - N_f) \times (N_\xi - N_f)}, \end{aligned} \tag{6}$$

where $\mathbf{H}_{ff}$, $\mathbf{H}_{fq}$, and $\mathbf{H}_{qq}$ represent the relation between faults, the relation between faults and uncertainty, and the relation between system uncertainty, respectively, while $N_f$ is the number of fault parameters in the system. Finally, the criterion is given by:

$$\Psi_{D_s}(\mathbf{H}_\xi) = N_l^{-1} \sum_{l=1}^{N_l} \log \left| \mathbf{H}_{ff}^{[l]} - \mathbf{H}_{fq}^{[l]} \left( \mathbf{H}_{qq}^{[l]} \right)^{-1} \mathbf{H}_{qf}^{[l]} \right|^{1/N_\xi}. \tag{7}$$

### *2.3 Inferential sensing*

Inferential sensors gather and combine information from other available system variables (or parameters) toward estimating a parameter of interest. Herein, they were designed to be particularly sensitive to faults and neglect the impact of uncertainty, thus granting superior detection capabilities.

We derived inferential sensors for the case of the closed loop system. These sensors combine information in $\hat{y}$ and $u_p$, to estimate the system fault level regardless of the existing uncertainty: $\hat{z}_c = g(\hat{y}, u_p(t))$. For scaling purposes, we normalize $\hat{z}_c$ with their nominal values, $\hat{z}_{c,nom} = g(\hat{y}_{nom}, u_{nom})$: $\bar{z}_c = \hat{z}_c / \hat{z}_{c,nom}$. The term $\hat{y}_{nom}$ denotes the nominal value of the system outputs, while $u_{nom}$ is the value of the system input when the system is in a healthy state.

To develop inferential sensors we conducted symbolic regression, by means of a genetic programming (GP) algorithm. The latter consists of a user-defined number of generations, in each of which a large number of relationships (i.e., population size) between $y$ and $u_p$ is generated. Then, the individual relationships were evaluated based on the $D_s$-optimality criterion as fitness function, which incorporates the sensitivity matrix of the inferential sensors $\mathbf{Q}_z$.

Based on the the principles of chain rule, it can be proved that the sensitivity matrix, $\mathbf{Q}_z$, for the inferential sensors is given by:

$$\mathbf{Q}_z = \frac{\partial \bar{z}}{\partial \boldsymbol{\xi}} = \frac{\partial \bar{z}}{\partial \hat{y}} \frac{\partial \hat{y}}{\partial \boldsymbol{\xi}} - K_P \frac{\partial \bar{z}}{\partial u_p} \frac{\partial \hat{y}}{\partial \boldsymbol{\xi}} + K_I \frac{\partial \bar{z}}{\partial u_p} \left[ \frac{\partial (\int_0^t e \, dt)}{\partial \boldsymbol{\xi}} \right]. \tag{8}$$

Given that $x_e(t) = \int_0^t e(t) \, dt$, Eq. 8 can be written differently as follows:

$$\mathbf{Q}_z = \frac{\partial \bar{z}}{\partial \boldsymbol{\xi}} = \frac{\partial \bar{z}}{\partial \hat{y}} \frac{\partial \hat{y}}{\partial \boldsymbol{\xi}} - K_P \frac{\partial \bar{z}}{\partial u_p} \frac{\partial \hat{y}}{\partial \boldsymbol{\xi}} + K_I \frac{\partial \bar{z}}{\partial u_p} \frac{\partial x_e}{\partial \boldsymbol{\xi}}. \tag{9}$$

The initial population in GP was generated randomly based on functions defined through knowledge of the governing physical processes and fault mechanisms. In the subsequent generations, the population underwent evolution, with fractions devoted to reproduction, crossover, and mutation. In the first generation, the individual with the maximum $D_s$-optimality criterion value was selected and maintained until a better one was obtained in the succeeding iterations. When the process was concluded, we obtained the optimal inferential sensor and employed it for fault detection.

In previous work (see Safikou and Bollas (2021)), we derived an inferential sensor for the open-loop system (i.e., the hard sensor $\hat{\mathbf{y}}$) through a Genetic Programming (GP) algorithm using symbolic regression. Again, the GP algorithm optimized the $D_s$-optimality criterion for the system model augmented with a symbolically regressed equation (i.e., the so-called inferential sensor); for further details, the reader is referred to Safikou and Bollas (2021). Note that, the derived soft sensor is a function of the hard sensors only, as $\bar{z}_o = m(\hat{\mathbf{y}})$. In this work, we adopt this optimal inferential sensor to assess its capability to provide real-time fault estimation in an open-loop system when combined with an EKF.

### *2.4 Extended Kalman Filter*

The Extended Kalman Filter (EKF) is an iterative method for estimating the states of a dynamic system based on a sequence of imprecise measurements. It represents an expansion of the classical Kalman Filter and is especially valuable when addressing systems with nonlinear characteristics.

In the field of fault detection, we augment the derivative state vector with auxiliary states that represent the fault parameters and we set their derivatives to zero. In this regard, the EKF performs state and fault estimation based on the measurements of the inferential sensors. The formulation of the EKF is provided in Table 1, where $\mathbf{q}_k$ and $\mathbf{r}_k$ are the covariances of the process and observation noises respectively. More details for the explanation and the formulation of the EKF can be found in Bar-Shalom et al. (2001).

## 3. CASE STUDY

We applied the proposed framework in a plate-fin cross-flow heat exchanger (PFHE) system described analytically in Palmer et al. (2016). The system input is the the mass flow rate of the hot stream, $u_p = \dot{m}_{h,i}$ (in kg/s), while the system outputs (i.e., the hard sensors) are the temperatures and pressures of the outlet streams, $\mathbf{y} = [T_c, T_h, P_c, P_h]$. In this work, the studied fault is the thermal fouling resistance in the cold stream, $\xi_f = R_f$.

For the development of the inferential sensors, we assumed four fault scenarios: (a) a fault-free scenario (i.e., $R_f = 0.4$), (b) 20% blocked fouling (i.e., $R_f = 1.6$), (c) 50% blocked fouling (i.e., $R_f = 4$), and (d) 80% blocked fouling (i.e., $R_f = 6.4$).

The parameter related to system uncertainty correspond to the cold air inlet stream moisture content, $\omega_{H_2O}$. Table 2

Table 1. EKF mathematical formulation

**Initialization**

$$\hat{\mathbf{x}}_{k-1|k-1} = E[\mathbf{x}(k-1)]$$

$$\mathbf{P}_{k-1|k-1} = E[(\mathbf{x}_{k-1|k-1} - \hat{\mathbf{x}}_{k-1|k-1})(\mathbf{x}_{k-1|k-1} - \hat{\mathbf{x}}_{k-1|k-1})^T]$$

**State Prediction**

$$\dot{\hat{\mathbf{x}}}_{k|k-1} = \mathbf{f}\left(\hat{\mathbf{x}}_{k-1|k-1}, \mathbf{u}_{p,k}, \boldsymbol{\theta}_p, \boldsymbol{\xi}_q, \boldsymbol{\xi}_f, t_k\right)$$

$$\dot{\mathbf{P}}_{k|k-1} = \mathbf{F}_k \mathbf{P}_{k-1|k-1} + \mathbf{P}_{k-1|k-1} \mathbf{F}_k{}^T + \mathbf{q}_k$$
$$\mathbf{F}_k = \frac{\partial f}{\partial x}$$

**Correction/Update**

$$\mathbf{K}_k = \mathbf{P}_{k|k-1} \mathbf{H}_k{}^T (\mathbf{H}_k \mathbf{P}_{k|k-1} \mathbf{H}_k{}^T + \mathbf{r}_k)^{-1}$$

$$\hat{\mathbf{x}}_{k|k} = \hat{\mathbf{x}}_{k|k-1} + \mathbf{K}_k(\hat{\mathbf{z}}_k - g(\hat{\mathbf{y}}_{k|k-1}, u_{p,k|k-1}))$$

$$\mathbf{P}_{k|k} = [(\mathbf{I} - \mathbf{K}_k \mathbf{H}_k)\mathbf{P}_{k|k-1}$$

$$\mathbf{H}_k = \frac{\partial g}{\partial x}$$

shows the probability distributions of system parameters, inputs, and outputs.

Table 2. System inputs, outputs and parameters, with their corresponding distributions.

| Uncertainty and Noise | Distribution |
|---|---|
| Cold Temperature, $T_c$ [C] | $\mathcal{N}(100, 0.05^2)$ |
| Hot Temperature, $T_h$ [C] | $\mathcal{N}(95, 0.05^2)$ |
| Moisture Content, $\omega_{\mathrm{H_2O}}$ | $\mathcal{N}(6, 0.5^2)$ |
| Input Space, $\mathbf{U}_p$ | [0.1, 1] |

For the case of the closed-loop system, the PI controller given by Eq. 10 aims to control the $y = [T_c]$ at the desired set value $y^* = 100$ $^o$C by manipulating the $u_p = \dot{m}_{h,i}$.

$$u_p(t) = 0.001e(t) + 0.0001 \int_0^t e(t)\, dt. \tag{10}$$

Note that the parameters $K_P$ and $K_I$ were tuned by using the trial and error method, until we reach a desirable controller performance.

The time series of the data corresponding to the fault scenarios provided to the GP algorithm, toward deriving an inferential sensor, are shown in Fig. 2. At the beginning ($t = 1500$ sec), the system is at steady-state in a healthy, fault-free, state without the existence of uncertainty. At $t = 2000$ sec, after the system has reached steady state, a step change can be noticed in the fault level to: i) 20% blocked, ii) 50% blocked, and iii) 80% blocked fouling. Note that, a case where the system remained in a healthy state was also included in Fig. 2.

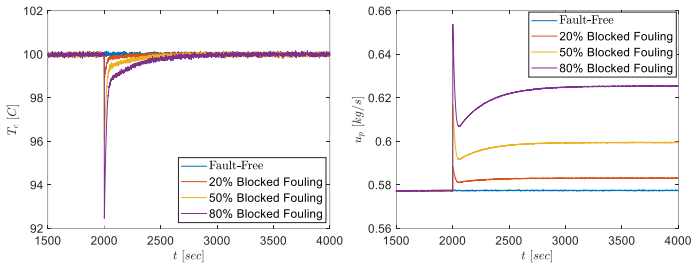


Fig. 2. The system responses, as well as the actuating signal performance, for the different fault scenarios.

For the fault scenarios of Fig. 2 and the timespan $\tau = [2001, 4000]$ sec, we trained the inferential sensor with the GP algorithm of Section 2.3. For the needs of symbolic regression, we employed the GPTIPS-2 toolbox; see Searson et al. (2010).

In the case of open-loop system, on the other hand, the inferential sensor was derived by incorporating in the GP the hard sensor model outputs, temperatures and pressures, at each fault scenario; see analytically in Safikou and Bollas (2021).

Two types of fault detection (FD) tests are examined in this work: i) Open-loop system FD test with duration of 300 sec, where two stepwise changes in $u_p$ and $\omega_{\mathrm{H_2O}}$ are observed at times 100 sec and 200 respectively; see Fig. 3(a-b), and ii) Closed-loop system FD test which lasts 1000 sec and a step change in $\omega_{\mathrm{H_2O}}$ can be noticed at time 50 sec as shown in Fig. 4(a), which led to manipulating $u_p$ as shown in Fig. 4(b). In both applications the fault level in the system is 50% blocked fouling (i.e., $R_f = 4$) and remains constant for the entirety of the test.

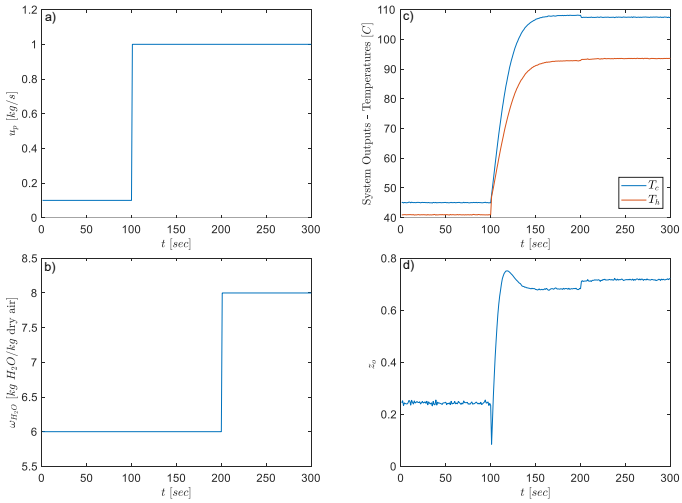


Fig. 3. Open-loop system FD test: a) the system input, b) the system uncertainty, c) the hard sensor data, and d) the inferential sensor data.

## 4. METHOD VERIFICATION AND COMPARISONS

Initially, we derive the inferential sensors by GP for both FD tests described in Section 3. The inferential sensor for the case of the open loop system is a function of both system temperatures that are provided in Fig. 3(c) and is given by Eq. 11. The response of $z_o$ for the timespan of 300 sec is presented in Fig. 3(d).

$$z_o = (-190.8T_c + 178.7T_h - 2T_c(-T_c + T_h + 6.6) + 1139.9)/(-1488.7) \tag{11}$$

Table 3. Estimates of the thermal fouling resistance obtained with EKF for the Open-loop and Closed-loop FD tests.

| FD Test | Fault Parameter: Thermal Fouling Resistance | Initial Guess | EKF Estimate with Hard Sensors | EKF Estimate with Inferential Sensors | True Value |
|---|---|---|---|---|---|
| Open loop system | $R_f \times 10^3$ m$^2$ K/W | 6.4 | 4.26 | 4.18 | 4 |
| Closed-loop system | $R_f \times 10^3$ m$^2$ K/W | 6.4 | 4.66 | 4.63 | 4 |

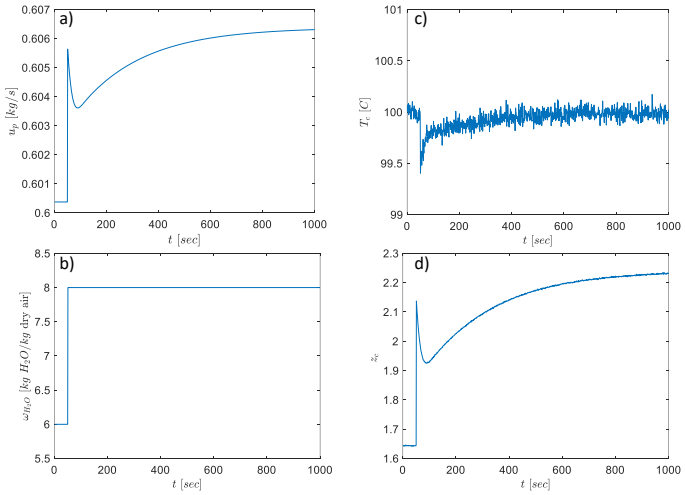


Fig. 4. Closed-loop system FD test: a) the system input, b) the system uncertainty, c) the hard sensor data, and d) the inferential sensor data.

The function of the obtained sensor for the closed-loop system, on the other hand, combines $u_p$ and $T_c$ and is expressed as follows:

$$z_c = [u_p + \log(u_p)]^4 \ [(u_p - T_c)^2 \ + (u_p \ \log(u_p)^2] + 1 \quad (12)$$

As we can see in Fig. 4(a,c), any system disturbance, i.e. a change in $\omega_{H_2O}$ that took place at $t = 50$, affects the controlled variable, $T_c$. To maintain and adjust $T_c$ to the desired set value of 100 $^o$C, $u_p$ was manipulated by the PI controller as indicated in Fig. 4(b). Fig. 4(d) shows the performance of $z_c$.

Then, we implemented an EKF for the estimation of system fault level based on the inferential sensor data (see Figs. 3(d) and 4(d)). For comparison purposes, we provided also the EKF estimates by incorporating the hard sensor measurements. (see Figs. 3(c) and 4(c)). The EKF performances during the timespans are shown in Figs. 5 and 6. In both figures, the EKF is able to estimate the fault level. One can notice that in the case of the open-loop system, the EKF estimates, either using the hard sensor or inferential sensor data, are closer to the true fault level, $R_f = 4$, (see Fig. 5) compared to the case of the closed-loop system (see Fig. 6).

Table 3 demonstrates in detail the initial guess, the true values of fault, as well as the estimates given by the EKF. The fault level for the open loop system is estimated at 4.18 considering the inferential sensor and at 4.26 by taking into consideration the hard sensor data. The estimated deviations of the true fault levels are 0.18 and 0.26 respectively. Along these lines, the inferential sensor provides a 8% improvement in fault estimation compared to the existing hard sensors in the case of the open loop systems.

In the case of the closed-loop system, on the other hand, the EKF with the inferential sensor data provided a fault estimate closer to the true value (i.e., 4.63), compared to the hard sensor data (i.e., 4.66). We observe that the estimate was improved by 3% with the use of the $z_c$ instead of the $T_c$.

Table 3 demonstrates that the accuracy of the EKF estimates significantly improves when incorporating the open-loop system compared to using closed-loop data, whether it's from inferential sensors or hard sensors. Notably, when integrating open-loop hard sensor data, we observed an 4% enhancement in fault estimation accuracy. Additionally, incorporating closed-loop inferential sensor data improved the estimates by 5%. This is reasonable, as in closed-loop systems the fault detection is more challenging, due to the controller masking the evidence of the fault.

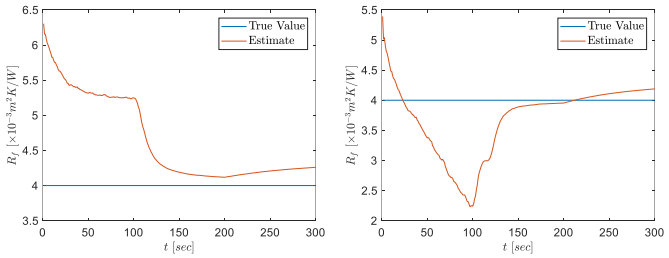


Fig. 5. The performance of the EKF when integrated with an open-loop system incorporating: a) the hard sensor measurements and b) inferential sensor measurements.

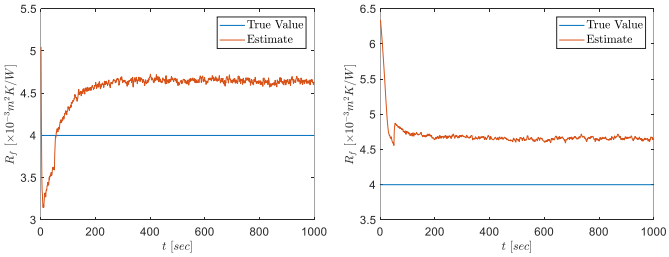


Fig. 6. The performance of the EKF when integrated with an closed-loop system incorporating: a) the hard sensor measurements and b) inferential sensor measurements.

## 5. CONCLUSION

We applied inferential sensing techniques and information theory to develop fault-sensitive soft sensors for both open-loop and closed-loop configurations in a PFHE (Plate Fin Heat Exchanger) system. By incorporating hard sensor data into a genetic programming algorithm, we created soft sensors, which were evaluated based on the $D_s$-optimality criterion, a measure derived from the Fisher

Information Matrix that quantifies fault information independently of system uncertainty and sensor noise. These soft sensors were then used to implement an Extended Kalman Filter (EKF) for fault level estimation in the PFHE system.

To assess the performance of the inferential sensors, we also estimated fault levels using the EKF with the existing hard sensor data. Our findings indicate that the inferential sensors provided more accurate estimates of the true fault level when compared to the existing hard sensors. Furthermore, when considering the open-loop system over the closed-loop system, regardless of the sensor data, the EKF estimates exhibited a notable 5% improvement.

## ACKNOWLEDGEMENTS

This work was supported by the Pratt & Whitney Institute for Advanced Systems Engineering (P&W-IASE) of the University of Connecticut. Any opinions expressed herein are those of the authors and do not represent those of the sponsor.

## REFERENCES

Andersson, J., Åkesson, J., and Diehl, M. (2012). CasADi: A symbolic package for automatic differentiation and optimal control. In *Lecture Notes in Computational Science and Engineering*, volume 87 LNCSE, 297–307. doi:10.1007/978 − 3 − 642 − 30023 − $3_2$7.

Atkinson, A.C. (2011). Optimum Experimental Design. In *International Encyclopedia of Statistical Science*, 1037–1039. Springer Berlin Heidelberg, Berlin, Heidelberg. doi:10.1007/978 − 3 − 642 − 04898 − $2_4$34.

Bar-Shalom, Y., Li, X.R., and Kirubarajan, T. (2001). *Estimation with Applications to Tracking and Navigation*. John Wiley & Sons, Inc., New York, USA. doi:10.1002/0471221279. URL `http://doi.wiley.com/10.1002/0471221279`.

Bokor, J. and Szabó, Z. (2009). Fault detection and isolation in nonlinear systems. *Annual Reviews in Control*, 33(2), 113–123. doi:10.1016/j.arcontrol.2009.09.001.

Boskovic, J.D., Li, S.M., and Mehra, R.K. (1999). Intelligent spacecraft control using Multiple Models, Switching, and Tuning. *IEEE International Symposium on Intelligent Control - Proceedings*, 84–89. doi:10.1109/isic.1999.796635.

Glavaški, S. and Elgersma, M. (2001). Diagnostics for active management of aircraft system failures. *IEEE Aerospace Conference Proceedings*, 7, 73179–73187. doi:10.1109/aero.2001.931394.

Harmouche, J., Delpha, C., and Diallo, D. (2014). Incipient fault detection and diagnosis based on Kullback-Leibler divergence using Principal Component Analysis: Part i. *Signal Processing*, 94(1), 278–287. doi:10.1016/j.sigpro.2013.05.018. URL `http://dx.doi.org/10.1016/j.sigpro.2013.05.018`.

Jihani, N., Kabbaj, M.N., and Benbrahim, M. (2023). Kalman filter based sensor fault detection in wireless sensor network for smart irrigation. *Results in Engineering*, 20, 101395. doi:https://doi.org/10.1016/j.rineng.2023.101395.

Lemos, A., Caminhas, W., and Gomide, F. (2013). Adaptive fault detection and diagnosis using an evolving fuzzy classifier. *Information Sciences*, 220, 64–85. doi:https://doi.org/10.1016/j.ins.2011.08.030. Online Fuzzy Machine Learning and Data Mining.

Livera, A., Phinikarides, A., Makrides, G., Sutterlueti, J., and Georghiou, G. (2017). Advanced failure detection algorithms and performance decision classification for grid-connected pv systems. doi:10.4229/EUPVSEC20172017-6BV.2.13.

Masdoua, Y., Boukhnifer, M., Adjallah, K.H., and Benterki, A. (2023). Fault detection and diagnosis in ahu system using deep learning approach. *Journal of the Franklin Institute*. doi:https://doi.org/10.1016/j.jfranklin.2023.09.046.

Maybeck, P.S. (1999). Multiple model adaptive algorithms for detecting and compensating sensor and actuator/surface failures in aircraft flight control systems. *International Journal of Robust and Nonlinear Control*, 9(14), 1051–1070. doi:10.1002/(SICI)1099-1239(19991215)9:14¡1051::AID-RNC452¿3.0.CO;2-0.

Mu, B., Yang, X., and Scott, J.K. (2022). Comparison of advanced set-based fault detection methods with classical data-driven and observer-based methods for uncertain nonlinear processes. *Computers & Chemical Engineering*, 166, 107975. doi:doi.org/10.1016/j.compchemeng.2022.107975.

Palmer, K.A. and Bollas, G.M. (2019). Active fault diagnosis for uncertain systems using optimal test designs and detection through classification. *ISA Transactions*, 93, 354–369. doi:10.1016/j.isatra.2019.02.034.

Palmer, K.A., Hale, W.T., Such, K.D., Shea, B.R., and Bollas, G.M. (2016). Optimal design of tests for heat exchanger fouling identification. *Applied Thermal Engineering*, 95, 382–393. doi:https://doi.org/10.1016/j.applthermaleng.2015.11.043.

Safikou, E. and Bollas, G.M. (2021). Sensor Fusion and Inferential Sensing for Fault Detection and Isolation in Uncertain Systems. *Conference on Control and Fault-Tolerant Systems, SysTol*, 2021-September, 85–90. doi:10.1109/SysTol52990.2021.9594985.

Searson, D.P., Leahy, D.E., and Willis, M.J. (2010). GPTIPS: An open source genetic programming toolbox for multigene symbolic regression. In *Proceedings of the International MultiConference of Engineers and Computer Scientists 2010*, volume 1.

Shamsuzzoha, M. (2013). Closed-loop PI/PID controller tuning for stable and integrating process with time delay. *Industrial and Engineering Chemistry Research*, 52(36), 12973–12992. doi:10.1021/ie401808m.

Sun, B., Wang, J., He, Z., Zhou, H., and Gu, F. (2019). Fault identification for a closed-loop control system based on an improved deep neural network. *Sensors (Switzerland)*, 19(9). doi:10.3390/s19092131.

Switzer, P., Harden, J.W., and Mark, R.K. (1988). A statistical method for estimating rates of soil development and ages of geologic deposits: A design for soil-chronosequence studies. *Mathematical Geology*, 20(1), 49–61. doi:10.1007/BF00903188.

Tan, M.K., Lee, K.L., Lim, K.G., Haron, A.R., Ibrahim, P., and Teo, K.T.K. (2021). Advanced fault detection in dc microgrid system using reinforcement learning. In *2021 IEEE International Conference on Artificial Intelligence in Engineering and Technology (IICAIET)*, 1–6. doi:10.1109/IICAIET51634.2021.9573711.